# Enhancing Functionalities in Nanocomposites for Effective Dye Removal from Wastewater: Isothermal, Kinetic and Thermodynamic Aspects

Ifrah Javed [1], Muhammad Asif Hanif [1], Umer Rashid [2,*], Farwa Nadeem [1], Fahad A. Alharthi [3] and Elham Ahmed Kazerooni [4]

1    Nano and Biomaterials Lab, Department of Chemistry, University of Agriculture, Faisalabad 38040, Pakistan
2    Institute of Nanoscience and Nanotechnology (ION2), Universiti Putra Malaysia, Serdang 43400, Selangor, Malaysia
3    Chemistry Department, College of Science, King Saud University, Riyadh 1145, Saudi Arabia
4    Department of Applied Biosciences, Kyungpook National University, Daegu 41566, Korea
*    Correspondence: umer.rashid@upm.edu.my or dr.umer.rashid@gmail.com; Tel.: +60-397-697-393

**Abstract:** The adsorption process combined with electrocoagulation is a highly effective technique for dye removal. Calcinized and non-calcinized composites based on bentonite and sodium zeolite were prepared for adsorptive removal of Foron EBL blue, Terasil brown 2RFL, Torque blue PG, and Orange $P_3R$ dyes. Factors affecting the adsorption process, such as contact time, initial dye concentration, and temperature, were also explored in this study. Equilibrium data of natural clay composites was explained by Freundlich, Langmuir, Dubinin Radushkevich isotherm, Harkin Jura, and Temkin isothermal models. Harkin Jura isotherm model best fitted on the adsorption mechanism compared to Langmuir and Temkin isotherm model. Morphology of clay-based adsorbents and functional group arrangement were investigated by scanning electron microscopy (SEM) and Fourier-transform infrared spectroscopy (FTIR). The calcinized nano-composite material exhibited better adsorption capacity than non-calcinized nano-composite and could be employed as a low-cost alternative for dye removal.

**Keywords:** composite material; Bentonite; zeolite; dyes; adsorption; SEM

## 1. Introduction

The world is facing wastewater pollution resulting from industrialization, urbanization, land use change, increased living standards, and wastewater management strategies [1]. Global wastewater discharge into the rivers, lakes, and seas reaches 400 billion $m^3$/year, polluting ~5500 billion $m^3$ of water annually [2]. In Pakistan, the textile industry has a high concentration of dye and releases more polluted and toxic wastewater than other industries [3]. Dye wastewater generally consists of a very large number of pollutants such as bases, acids, dissolved solids, toxic compounds, and color [4]. Discharge of dye effluents without proper treatment could badly impact soil, ecosystems, and water bodies because they are carcinogenic and poisonous. This textile wastewater contributes about 17–20% of wastewater pollution, according to the World Bank [5]. Therefore, dye removal before disposal into the wastewater is very necessary, and suitable methods are desired for the purification of wastewater [6].

Various chemical and physical techniques have been applied for dye treatment, including ozonation, coagulation, flocculation, ultrasound irradiation, and photocatalysis. These processes have environmental and economic drawbacks, such as sludge production, operating cost, and complexity of treatment procedure [7,8]. The adsorption process in all these techniques offers the best potential for dye removal due to economic reasons. The adsorption procedure may produce utile or no toxic pollutants. Furthermore, it has

no environmental issues, yields treated water of high quality, and does not generate any sludge [9]. A combination of different procedures in effluents treatment shows superior removal efficiencies for dye removal than a single treatment [10]. In this project, two sequential treatments, the adsorption and electrocoagulation process, have been planned for wastewater treatment. The Electrocoagulation method is a very reliable, low-cost, simple, and efficient technique for dye removal. No additional chemicals are needed for applications. This technology requires an electrical current of very low intensity and can be operated using green processes, such as windmills, fuel cells, and solar cells [11]. EC technique uses the sources of direct current by using different electrodes, which are immersed for removal purposes in polluted water [12].

Natural and modified clay minerals are extensively used as low-cost adsorbents due to their abundant accessibility. Bentonite is one of the most widely used adsorbents among these clay minerals [13]. Bentonite (BT) is made up of at least 50% smectite and, more precisely, montmorillonite, and it is a layered silicate clay mineral. Hydrated aluminum silicate is another name for this substance. Isometric trapezohedron in its structure has a large central open area, ions, and other molecules which can pass through this framework (Rulli). Recently, different techniques have been discussed for preparing cost-effective novel composites as adsorbents for dye removal [14–16]. Composites combine two or more materials in a specific manner and enhance treatment efficiency. They exhibit customized characteristics and large potential compared to their individual components [17].

The present study describes the novel and low-cost composite materials of bentonite and sodium zeolite that have been used to remove Reactive Orange $P_3R$, disperse dye Terasil Brown 2RFL, Torque blue PG, and Foron EBL blue dyes.

## 2. Materials and Methods

### 2.1. Materials

Foron EBL blue, Torque blue PG, Terasil brown 2RFL, and Orange $P_3R$ dyes were obtained from the dyeing industry, Faisalabad. Bentonite clay (500 g) in the form of stone and sodium zeolite (250 g) were also purchased in powder form from the local market of Faisalabad city. All chemical reagents in this study, including 0.1 M dil. HCl solution, 0.1 M NaOH, Nitric acid, and Buffer solution of 7 pH were of analytical grade. Distilled water was used for the preparation of required solutions.

### 2.2. Spectrophotometric Analysis

Solutions of all 4 dyes (Foron EBL blue, Torque blue PG, Terasil brown 2RFL, and Orange $P_3R$) were prepared by dissolving 0.001 g of each dye in 40 mL distilled water to prepare a 25 ppm dye solution. Spectrophotometric analysis of dye solutions was performed using a 721 D UV visible spectrophotometer to find the maximum wavelength $\lambda_{max}$ of each dye. Absorbance was monitored at the 380–800 nm wavelength range for analysis [18].

### 2.3. Preparation of Bentonite

Bentonite clay was used as a starting material to prepare bentonite/zeolite composite. Clay stone was crushed and sieved to obtain desired particle size. Bentonite sample was prepared by performing filtration. Excess water was added to clay and filtered using the Whatman filter paper. Filtration helped to purify the clay by removing the non-clay materials such as non-soluble salts, minerals, and non-suspended particles of clay [19]. After filtration, purified clay filtrate in paste form was dried at room temperature. This dried powder bentonite was used to produce composite material.

### 2.4. Preparation of Composite Materials

Calcinized and non-calcinized composite materials were prepared by purified bentonite and sodium zeolite. The non-calcinized composite was prepared by mixing sodium zeolite and bentonite in the distilled water with continuous stirring to obtain a fine paste

which was further dried at 60 °C in the oven. For the preparation of calcinized composite, a paste of bentonite and sodium zeolite was prepared in the same way, and calcination of the mixture was performed using a muffle furnace (range 30–3000 °C) at 750 °C for 4 h in Hitech Lab, University of Agriculture, Faisalabad.

*2.5. Adsorption Study*

The adsorption process of calcinized and non-calcinized composite materials was performed by agitating the composites with dye solutions using an orbital shaker at 120 rpm speed for 3 h. Dye solutions of Foron ebl blue, Torque blue PG, Terasil brown 2RFL, and Orange $P_3R$ were prepared with a molar concentration of 25 ppm, and the pH of the dye solutions was adjusted separately using 0.1 M NaOH and 0.1 M HCl solutions. A composite dosage (0.01 g) was added to each dye solution.

*2.6. Electrocoagulation*

Electrocoagulation was performed with adsorption process using different electrodes. Electrocoagulation combined with adsorption phenomenon has also been previously studied for cation and anionic dyes removal [10]. Initially, single electrodes of aluminium, copper, graphite and silver were used. But optimum results were obtained by using the combination of silver and copper electrodes. We have extended the further experiment using this combination. Copper and silver electrodes were put inside the dyes solution in such a way that their terminals cannot touch each other, now connect the electrodes with battery or solar panels to provide a 12 v current for 15–20 min.

Estimation of Absorbance and TDS

Water quality parameters such as TDS (total dissolved solvents) values and absorbance of all 4 dyes solutions were calculated using a TDS meter and 721 D UV-visible spectrophotometer, respectively. These values were measured before and after the electrocoagulation process to know the effect of adsorbent and electrocoagulation on dyes. Syringe filtration was used to filter the dye solutions to remove the adsorbent present in the solutions [20]. Solutions of dyes are taken in cuvettes and placed in a spectrophotometer to find their absorbance value at their maximum wavelength [18].

*2.7. Optimization of Initial Dye Concentration*

The effect of the initial dye concentration by varying the concentrations of dye from 5–50 mg/L was investigated for 4 dyes by keeping temperature, composite adsorbents dose, and contact time constant. In the orbital shaking process, time and shaking speed were 3 h and 120 rpm for this study, respectively. Electrocoagulation was also performed for each concentration for both calcinized and non-calcinized composites. To examine the relationship between adsorbent and dye concentration, different adsorption isotherms were tested.

Adsorption Isotherms

This isotherm describes how adsorbate interacts with the adsorbent and is critical in optimizing adsorbent usage. The applied isotherms to data were Langmuir Isotherm based on single layer coverage of adsorbate molecules [21], Freundlich Isotherm that assumes the energetic surface heterogeneity [22], Dubinin Radushkevich Isotherm used to exhibit adsorption mechanism using Gaussian energy distribution on the heterogeneous surface [22,23], Temkin Adsorption Isotherm that considers many exchanging sites onto the surface of the adsorbent, and Harkin–Jura Isotherm Model which demonstrates the heterogeneous distribution of pores and used to describe multi-layered adsorption phenomena [23].

## 2.8. Optimization of Contact Time

Solutions of dyes with two composites (calcinized and non-calcinized) were agitated for the different time intervals (30, 60, 90, 120, and 180 min). The experiments were conducted at 7 pH, and the adsorbent dose was kept constant (0.005 g) in all dye solutions. Electrocoagulation of all dye solutions was also performed for each shaking time interval (5, 10, 15, 20, and 30 min) to investigate the electrocoagulation time effect on the dye's removal. Kinetic data were examined using pseudo-first-order and pseudo-second-order kinetic models [23,24].

## 2.9. Optimization of Temperature

To analyze temperature effect on the decolorization of dyes, a series of experiments were conducted at temperatures ranging from 30 to 55 °C at the constant pH 7, adsorbent dose (0.005 g/L), and contact time of 3 h. For this purpose, dye solutions having composite materials were processed in an incubator at each temperature, and absorbance was measured before and after the electrocoagulation procedure. The thermodynamic reaction of adsorption is described via thermodynamic parameters, such as changes in Gibbs free energy ($\Delta G°$), changes in entropy $\Delta S^o$, and Enthalpy $\Delta H^o$. They explain the spontaneity, feasibility, and nature of adsorbate-adsorbent interactions. Parameters can be calculated from thermal data of adsorption of four dyes using the following equation.

$$\Delta G^o = \Delta H^o - T\Delta S^o$$

The linearized form of the Van't-Hoff equation is:

$$lnK_c = -\frac{\Delta H^o}{RT} + \frac{\Delta S^o}{R}$$

$K_c$ is the equilibrium constant and describes the ratio of the equilibrium concentration of dyes on the adsorbent to the equilibrium concentration of dyes in solution. $R$ is the ideal gas constant (8.314 J mol$^{-1}$ K$^{-1}$), and $T$ is used for adsorption temperature in Kelvin. $lnK_c$ versus $1/T$ plot should give a linear line. Values of $\Delta H°$ (J mol$^{-1}$), $\Delta S°$ (J mol$^{-1}$ K$^{-1}$), and Gibbs free energy ($\Delta G°$) are calculated by slope and intercept of van't Hoff plots [25].

## 2.10. Characterization of Adsorbents

The surface morphology of composites was studied using a scanning electron microscope (SEM) (Nova Nano SEM 450, FEI, Hillsboro, OR, USA) at 25,000 magnification. SEM analysis gives information about images of the clay type by scanning it using a focused beam of electrons [26]. In this study, this analysis was carried out using TLD and ETD detectors, and Specimens were observed in a high vacuum at 25,000× magnification in the micrometer range. The functional group arrangement was determined by Fourier-transform infrared spectroscopy (FTIR) (Spectrum Two, Perkin Elmer, Waltham, MA, USA) with a scanning range of 400–4000 cm$^{-1}$.

## 3. Results and Discussion

### 3.1. Determination of Maximum Wavelength ($\lambda_{max}$)

Spectrophotometer analysis measures how much chemical material absorbs the light by measuring the light intensity as a light beam passes to the sample solution. This analysis by using a 721 D UV/Vis spectrophotometer was performed for all four dye solutions to find out their maximum wavelength at 25 ppm concentration.

Absorbance measurements of standard solutions of all four dyes were performed at the 380–800 nm wavelength range. As shown in Figure 1, the maximum wavelength ($\lambda_{max}$) of Foron EBL blue dye at 25 ppm is 550 nm. Maximum wavelengths of Torque blue PG, Terasil brown 2RFL, and Orange P$_3$R dyes at 25 ppm analyzed by spectrophotometer were 620 nm, 470 nm, and 430 nm, respectively.
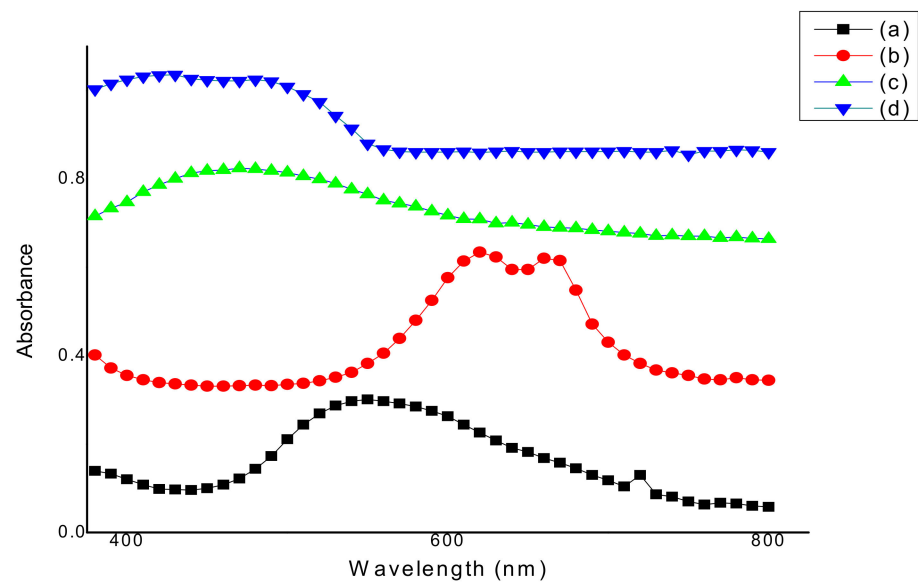
**Figure 1.** Graphical representation of spectrophotometric analysis of (**a**) Foron EBL blue, (**b**) Torque blue PG, (**c**) Terasil brown 2RFL, and (**d**) Orange $P_3R$ dye before treatment.

### 3.2. Effect of Calcination on Adsorption Capacity

Foron EBL blue dye, Terasil brown 2RFL, Orange $P_3R$, and Torque blue PG dye solutions were treated with calcinized and non-calcinized composites using adsorption and electrocoagulation processes. The decolorization efficiency of both composites was analyzed spectrophotometrically by examining absorbance values at the maximum wavelength of each dye before and after electrocoagulation. The total percentage degradation of all four dyes was obtained by the following formula:

$$\%Removal = (C_o - C_e) \times 100/C_o$$

Here, $C_o$ is the concentration of the dye in control without the adsorbent, and $C_e$ is the concentration of dye containing clay adsorbents [27].

As shown in Figure 2, non-calcinized bentonite and sodium zeolite composite exhibited 52.73% maximum removal of Terasil brown 2RFL. Calcinized bentonite and sodium zeolite composite have maximum Terasil brown 2RFL removal up to 86.68%. The results obtained show that on calcination, the adsorption capacity of clay composites significantly improved. In the calcination process, the ore is heated below the melting point to drive off moisture, volatile expunges, organic matter, and water of hydrates. Resultantly, calcinized composite has increased pore size and adsorption site. Ultimately, this material has a significantly higher adsorption capacity [28]. Similar results were exhibited by calcinized $ZnFe_2O_4$/Na-bentonite composite, which adsorbed more than 40% of Rhodamine B dye (RhB). Adsorption of RhB on unmodified pure clay composite was less than 20%. It is most likely due to the excellent capacity of adsorption and the large number of adsorption sites in composite [29]. Another study with calcinized bentonite clay for Rhodamine B dye adsorption showed similar results. Calcination treatment improved the mechanical properties, loss of hydration water, and reduced the surface area. Consequently, the adsorption efficiency of calcinized clay increased [30].
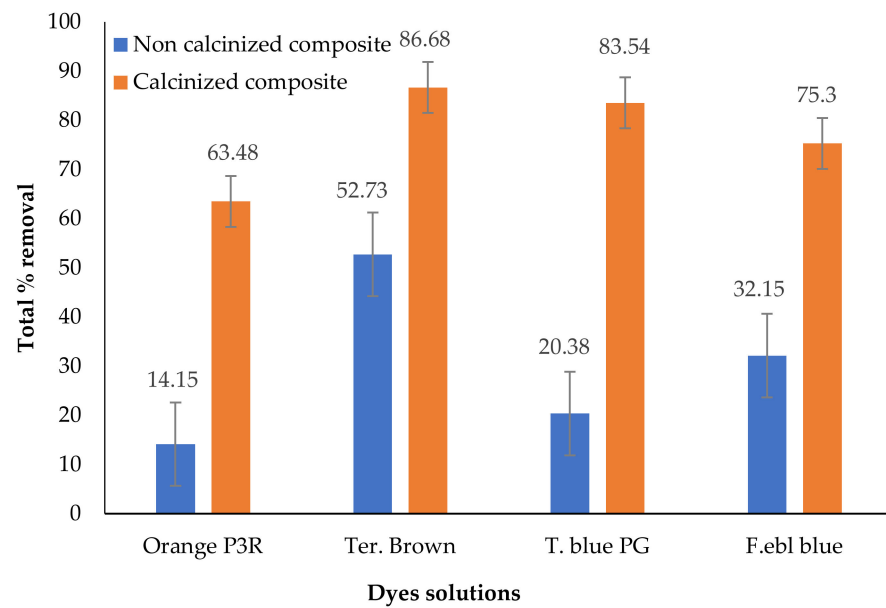
**Figure 2.** Percentage removal of Foron ebl blue, Terasil brown, Orange P$_3$R, and Torque blue dyes using calcinized and non-calcinized composites.

### 3.3. Effect of Electrocoagulation-Adsorption on Total Dissolved Solids (TDS)

Total Dissolved Solids (TDS) measures the combined content of organic and inorganic substances in liquid, ionized, or micro-granular (colloidal sol) ended form. It is used as an indication of the aesthetic characteristics of the drinking water, and electrocoagulation helps to remove these impurities [31]. The electrocoagulation process performed for only 15 min resulted in a significant decrease in water TDS. Afterward, using TDS electrocoagulation treatment, the same water sample was subjected to an adsorption process on clay composites. It further reduces TDS. TDS results are shown in Figure 3. Similar results were obtained in the treatment of industrial wastewater using the electrocoagulation method. To decrease the value of TDS, the best-used potential was 12 V. The effectiveness of the electrocoagulation method in decreasing the TDS values was 17.243% [32].
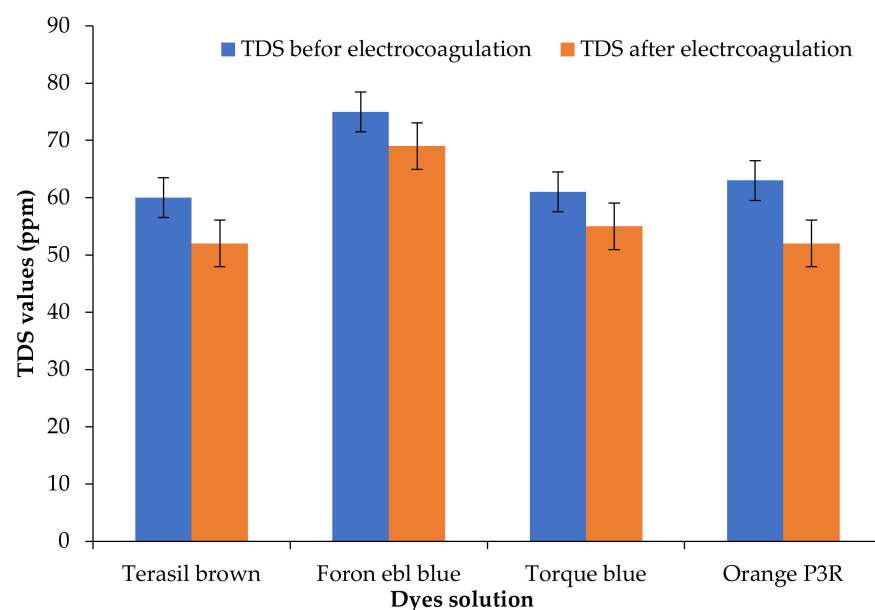


**Figure 3.** TDS values using clay composites before and after electrocoagulation.

### 3.4. Effect of Initial Dye Concentration

Effect of concentration of Foron ebl blue, Torque blue PG, Terasil brown, and Orange P$_3$R dyes was investigated for calcinized and non-calcinized composites. Initial concentrations of four dyes were varied to 5, 10, 20, 25, and 50 ppm. By increasing the initial concentration, the amount of dye adsorbed at equilibrium (q$_e$) increased sharply for both clay composites at a constant temperature, pH, time, and adsorbent dose.

Figure 4 shows the initial concentration effect on the adsorption capacity of composites towards all four dyes. This concentration gives the necessary driving force to overcome the resistance to the mass transfer of dye between the aqueous and the solid phase. By increasing concentration, the driving force also increases and enhances the dye diffusion rate [33]. Higher adsorption at the high initial dye concentrations is probably due to the saturation of active adsorption sites on the surface of the adsorbent takes place [34]. The trend of similar results in the adsorption performance has been reported for brilliant green cationic dye (BG) by Cellulose/Bentonite-Zeolite composite. Adsorption of BG (per unit mass) using initial dye concentrations of 50–200 mg/L increased (20.710–89.770 mg/g) with the increasing dye contents due to improvement of the driving force (concentration gradient). The rise in adsorption is due to the intensification in mass transfer at a higher initial dye concentration [35].
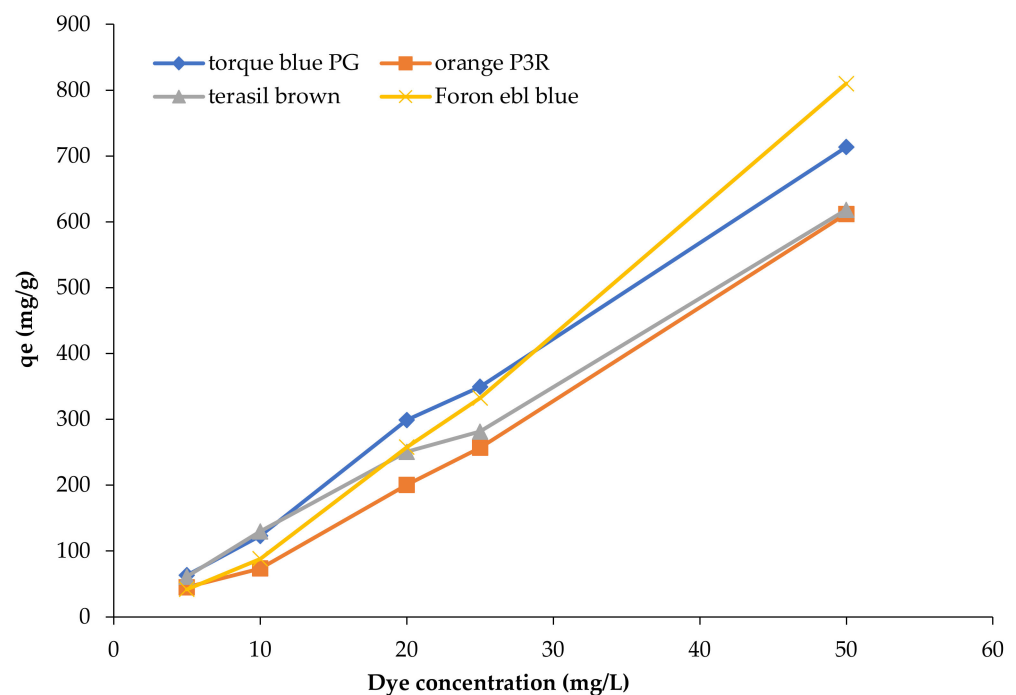


**Figure 4.** Effect of dye concentration on adsorption capacity of clay-based composites for dye removal.

### 3.5. Adsorption Modelling

Adsorption of dyes onto clay-based composites was examined using Langmuir, Dubinin Radushkevich, Freundlich, Temkin, and Harkin Jura isotherm models. Adsorption equilibrium studies demonstrate adsorbent capacity and studies adsorption isotherm using constants; their values show surface properties and affinity of adsorbents.

Resultant data of all model parameters using non-calcinized and calcinized clay composite are listed in Tables 1 and 2. Figures 5–9 for the fitting of the adsorption model related to Table 1 are also shown in this section. According to the regression coefficient (R$^2$), dyes adsorption on both clay composites was favorable for Freundlich, Dubinin Radushkevich, and Harkin Jura adsorption isotherms under the experimental conditions. Harkin Jura isotherm best described the uptake of dyes by linear analysis onto clay composites. Since the R$^2$ value nearer to 1 or R$^2$ > 0.9 indicates that the equation better fits the experimental

data [33]. The adsorptive behavior of dyes suggested the effective multilayer adsorption and the heterogeneous distribution of the active sites on bentonite and sodium zeolite-based adsorbents' surface. For all the concentrations, Temkin and Langmuir isotherms represented the poor fit of the experimental data in comparison with other isothermal equations. Freundlich constant $K_f$ indicates the adsorption capacity of the adsorbent, such as a greater $K_f$ value, having greater adsorption capacity. The magnitude of *n* represents the measure of favourability for adsorption. If *n* is equal to unity, then adsorption is linear. Moreover, *n* above unity represents favorable and physical adsorption. Adsorption energy (E) from the Dubinin Radushkevich model was found to be between ranges of 0.25 and 0.71 kJ/mol for clay composites, revealing the contribution of Physiosorption in dyes adsorption [36]. Similar results were obtained in adsorption of Rhodamine B dye, $Cd^{2+}$ and $Cu^{2+}$ ions by low-cost clay adsorbent and wheat straw. Linear plots of equilibrium isotherms represented that adsorption of Rhodamine B dye obeys the Freundlich adsorption model, suggesting the multilayer phenomenon [37]. In another study, the Harkin-Jura isotherm model represented a better fit to adsorption data than Freundlich and Temkin isotherms for reactive black 5 dye removal from wastewater using bentonite clay [38].

**Table 1.** Parameters obtained from different isothermic models using non-calcinized composites at 5, 10, 20, 25, and 50 ppm concentrations.

| Isotherm Models | Foron Ebl Blue Dye | Terasil Brown Dye | Orange P$_3$R | Torque Blue PG Dye |
|---|---|---|---|---|
| **Langmuir** | | | | |
| $q_{max}$ (mg/g) (cal) | 111.11 | 112.30 | 150 | 104.07 |
| $q_{max}$(exp) | 747.4408 | 778.688 | 571.688 | 873.4896 |
| $K_L$ (L/mg) | 0.0179 | 0.0103 | 0.047 | 0.0081 |
| $R^2$ | 0.4022 | 0.1745 | 0.026 | 0.2483 |
| **Fruendlich** | | | | |
| $q_{max}$ (cal) (mg/g) | 95.509 | 192.623 | 180.517 | 196.55 |
| $q_{max}$ (exp) | 747.44 | 788.688 | 571.688 | 878.48 |
| $R^2$ | 0.9585 | 0.7108 | 0.7939 | 0.9482 |
| $K_f$ (L/mg) | 3.18 | 1.118 | 0.037 | 1.426 |
| N | 2.075 | 2.109 | 1.3648 | 0.868 |
| **Dubinin-Radushkevich** | | | | |
| $q_o$ (mg/g) cal | 149.54 | 647.36 | 123.74 | 617.88 |
| $q_o$ (exp) | 747.44 | 788.688 | 571.688 | 878.48 |
| $\beta$ (mol$^2$/J$^2$) | 1.4185 | 0.8472 | 0.8193 | 0.695 |
| $R^2$ | 0.7268 | 0.9289 | 0.4297 | 0.9053 |
| E (KJ/mol) | 0.419 | 0.5432 | 0.55239 | 0.5997 |
| **Temkin isotherm** | | | | |
| B | 112.59 | 146.04 | 148.94 | 159.99 |
| $R^2$ | 0.7932 | 0.7765 | 0.5526 | 0.8063 |
| $A_t$ (L/g) | 0.5774 | 1.1753 | 0.5545 | 2.464 |
| **Harkin Jura isotherm** | | | | |
| $R^2$ | 0.9931 | 0.5775 | 0.9735 | 0.9592 |
| A | 333.3 | 703 | 412 | 500 |
| B | 0.099 | 0.1 | 0.15 | 0.5 |

**Table 2.** Adsorption isotherm parameters for all four dyes by calcinized composite at five different concentrations (5, 10, 20, 25, and 50 ppm).

| Isotherm Models | Foron Ebl Blue Dye | Terasil Brown Dye | Orange P$_3$R | Torque Blue PG Dye |
|---|---|---|---|---|
| **Langmuir** | | | | |
| $q_{max}$ (mg/g)(cal) | 109.89 | 85 | 151.51 | 175.33 |
| $q_{max}$(exp) | 810.13 | 618.48 | 612.204 | 713.57 |
| $K_L$ (L/mg) | 0.0214 | 0.0206 | 0.0037 | 0.0167 |
| $R^2$ | 0.8425 | 0.7665 | 0.5251 | 0.4608 |
| **Fruendlich** | | | | |
| $q_{max}$ (cal) (mg/g) | 125.81 | 136.3699 | 223.738 | 218.68 |
| $q_{max}$(exp) | 810.13 | 618.48 | 612.204 | 713.57 |
| $R^2$ | 0.8932 | 0.9795 | 0.9402 | 0.9536 |
| $K_f$ (L/mg) | 2.6503 | 5.156 | 8.994 | 3.0704 |
| N | 1.037 | 1.0548 | 0.738 | 0.828 |
| **Dubinin-Radushkevich** | | | | |
| $q_o$ (mg/g)cal | 145.65 | 363.72 | 283.36 | 617.099 |
| $q_o$ (exp) | 810.13 | 618.48 | 612.204 | 713.57 |
| $\beta$ (mol$^2$/J$^2$) | 4.6532 | 1.6845 | 3.21911 | 1.6933 |
| $R^2$ | 0.7268 | 0.9287 | 0.7297 | 0.9143 |
| E (KJ/mol) | 0.2318 | 0.3852 | 0.2786 | 0.3842 |
| **Temkin isotherm** | | | | |
| B | 130.83 | 117.83 | 162.4 | 114.67 |
| $R^2$ | 0.7773 | 0.8543 | 0.7333 | 0.8907 |
| $A_t$ (L/g) | 0.5125 | 0.4791 | 0.1972 | 0.0222 |
| **Harkin Jura Isotherm** | | | | |
| $R^2$ | 0.9411 | 0.713 | 0.9035 | 0.9386 |
| A | 416.66 | 500 | 333.3 | 166.67 |
| B | 0.916 | 0.15 | 0.1 | 0.116 |
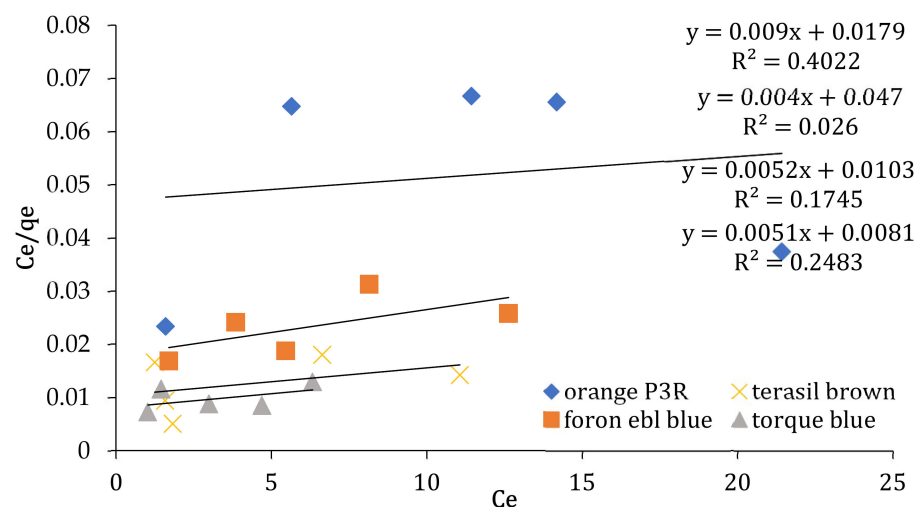


**Figure 5.** Langmuir isotherm at 5, 10, 20, 25, and 50 ppm concentrations for non-calcinized composite.
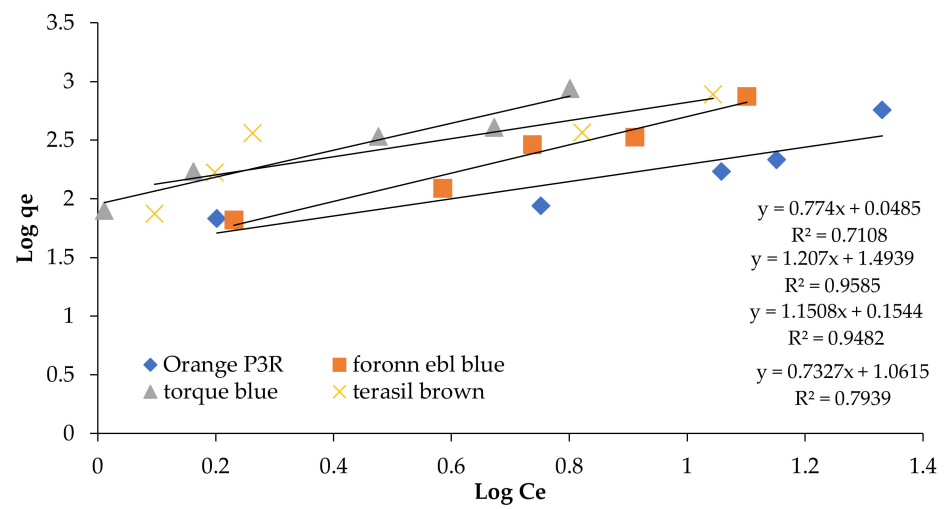
**Figure 6.** Fruendlich Isotherm at 5 concentrations for non-calcinized composite.
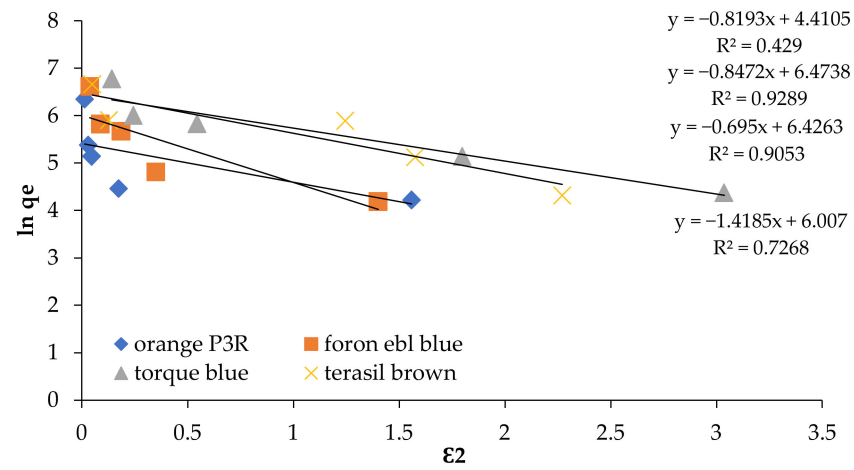


**Figure 7.** Dubinin Radushkevich Isotherm at 5 concentrations for non-calcinized composite.
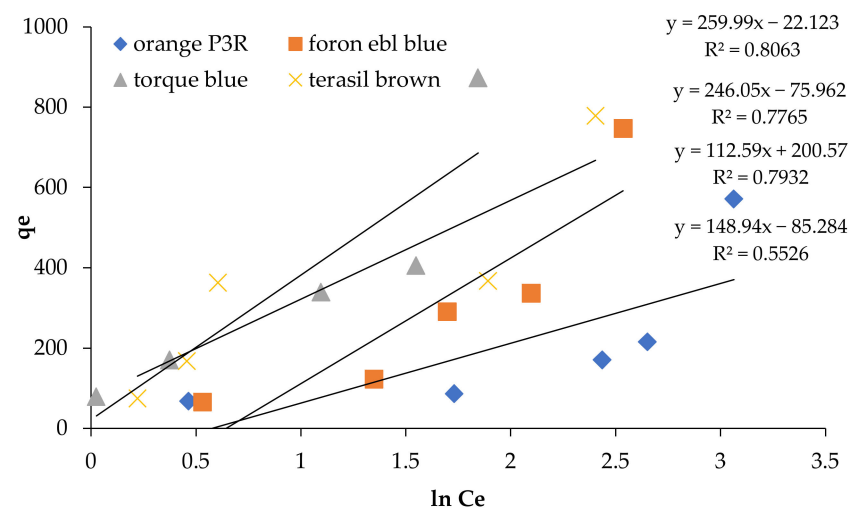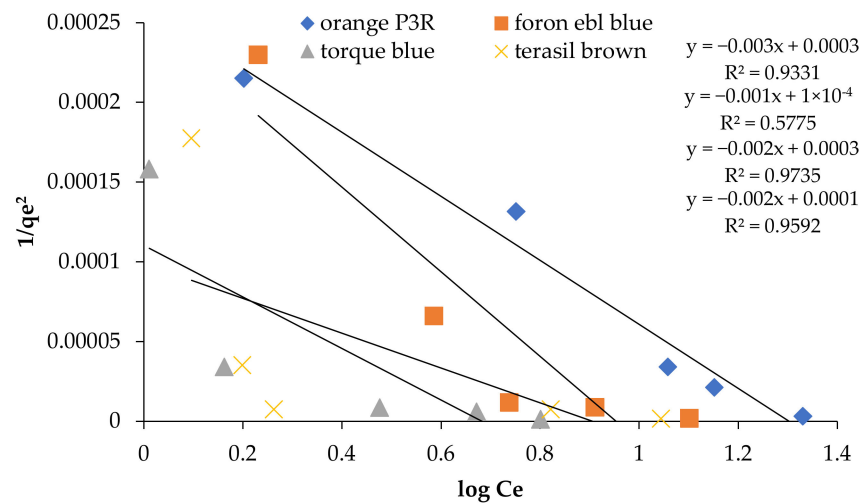


**Figure 8.** Temkin Isotherm at 5 concentrations for non-calcinized composite.

**Figure 9.** Harkin Jura Isotherm at 5 concentrations for non-calcinized composite.

*3.6. Effect of Time Contact*

The effect of contact time on the adsorption of four dyes from their aqueous solutions was explored at varying times from 30 to 180 min using a shaking process at 120 rpm for calcinized and non-calcinized composites. After each shaking time interval, electrocoagulation was performed at time intervals of 5, 10, 15, 20, and 30 min, and absorbance was measured. The adsorption capacity of composites for all dyes increases sharply with the prolongation of time initially; the uptake rate slows down over time (Figure 10).
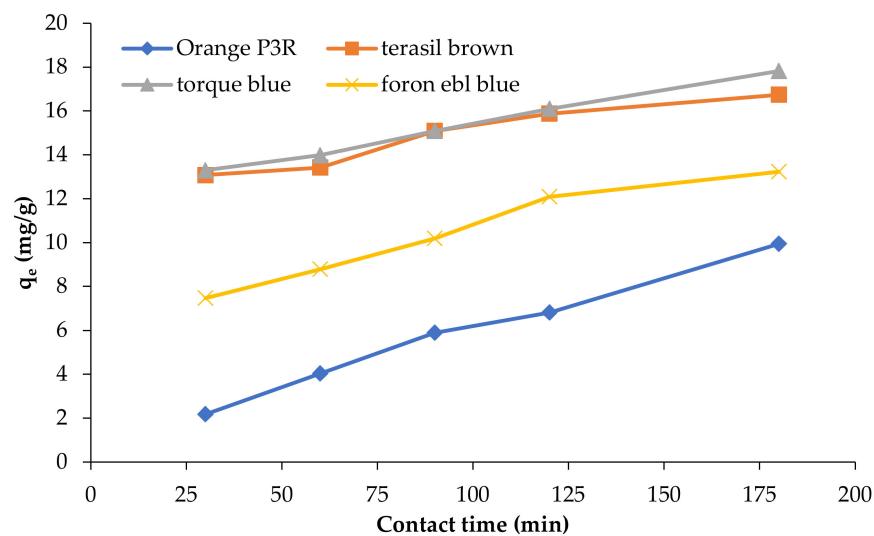


**Figure 10.** Effect of contact time on adsorption capacity ($q_e$) of composite materials for dye removal.

Rapid initial adsorption is due to the contacts of dye molecules with available adsorption sites at the surface. Following gradual adsorption may be attributed to the uptake of dyes into adsorbents pores. When binding sites become exhausted, the uptake rate of dyes slows down, and the chance for the availability of active sites decreases. Inorganic composite materials are dependable for a randomized pattern of adsorption [36]. The adsorbent was regenerated by heating at 750 °C for 4 h without any loss of adsorption capacity studied for five regeneration cycles.

*3.7. Kinetic Studies*

Pseudo-first/second-order kinetic models were used to investigate adsorption mechanism, potential rate controlling steps, chemical reaction, mass transfer, and dye adsorption

kinetics onto clay-based composites [25,39]. A comparison between Lagergren pseudo-first and pseudo-second-order kinetic models is tabulated in Table 3 for non-calcinized composite, and Table 4 shows the kinetic data using calcinized composite. According to the obtained results, the pseudo-second-order kinetic model was best fitted to all four dyes for both non-calcinized and calcinized composites, considering its high $R^2$ values ($R^2 > 0.9$). Estimated values of adsorption capacities ($q_e$) agreed with the experimental values ($q_e$-exp) using a pseudo-second-order kinetic model at all the time intervals. The Lagergren first-order kinetic model failed to describe the rate constant ($k_{1,ads}$) and $q_e$ of the model. Since experimental values differed from estimated and regression coefficient ($R^2$) values were lower, assuming that the adsorbate molecule is attached to the one binding site [39]. Using a non-calcinized composite, maximum adsorption values for Foron ebl dye were obtained after 180 min of shaking and 30 min of electrocoagulation, while Orange $P_3R$, Terasil brown 2RFL, and Torque blue PG dyes showed maximum absorption after 120 min of shaking and 30 min of electrocoagulation. The results showed a quick increase of adsorption capacity at the start and then a slow down with time. It is due to the accessibility of a large number of empty active binding sites for dye anions at the start of the adsorption process, and the process gradually slows with the coverage of vacant sites. Therefore, no maximum adsorption value was obtained after 180 min of shaking [40]. Calcinized composite shows better adsorption capacity than non-calcinized composite due to more adsorption sites and its increased surface area. Maximum adsorption values for Foron ebl dye, Terasil brown, and Torque blue PG were obtained after 90 min of shaking and 30 min of electrocoagulation. Orange $P_3R$ showed maximum adsorption at 120 min of shaking using a calcinized composite because photocatalytic efficiency increases due to the remaining silica-aluminates framework structures of zeolite and better crystallinity [41]. Applicability of the pseudo-second-order kinetic model implied that the adsorption occurs on the energetically heterogeneous surface of composite materials [42–44].

**Table 3.** Pseudo-first-order kinetics and Pseudo-second-order kinetics parameters of all four dyes at electrocoagulation time intervals (5, 10, 15, 20, 30 min) after a shaking period (30, 60, 90, 120, 180 min) using non-calcinized composite.

| Dyes | Pseudo First Order Kinetics | | | Pseudo Second Order Kinetics | | | |
|---|---|---|---|---|---|---|---|
| | $q_e$ (mg/g) Cal | $K_{1,ads}$ | $R^2$ | $q_e$ (mg/g) exp | $q_e$ (mg/g) | $K_{2,ads}$ | $R^2$ |
| Electrocoagulation time intervals after 30 min | | | | | | | |
| Foron ebl blue | 4.637565 | 0.05893 | 0.7957 | 12.1187 | 13.5318 | 0.022636 | 0.9918 |
| Terasil brown | 5.807644 | 0.06813 | 0.8063 | 18.0032 | 18.60784 | 0.020365 | 0.9964 |
| Orange $P_3R$ | 16.11759 | 0.08931 | 0.8752 | 12.70712 | 21.72727 | 0.00556 | 0.9525 |
| Torque blue | 2.736529 | 0.05639 | 0.89 | 17.9484 | 19.08397 | 0.024481 | 0.9957 |
| Electrocoagulation time intervals after 60 min | | | | | | | |
| Foron ebl blue | 2.782915 | 0.04235 | 0.7365 | 11.617 | 12.42236 | 0.035351 | 0.9964 |
| Terasil brown | 5.82908 | 0.06169 | 0.877 | 19.068 | 19.40816 | 0.020867 | 0.9964 |
| Orange P3R | 11.55846 | 0.08356 | 0.8606 | 12.244 | 18.01802 | 0.007998 | 0.9322 |
| Torque blue | 3.624933 | 0.04880 | 0.8571 | 19.1793 | 20.048 | 0.031247 | 0.998 |
| Electrocoagulation time intervals after 90 min | | | | | | | |
| Foron ebl blue | 1.695509 | 0.032228 | 0.3254 | 12.3336 | 12.87001 | 0.054284 | 0.9988 |
| Terasil brown | 2.200392 | 0.038213 | 0.5002 | 18.6022 | 19.19386 | 0.046535 | 0.9993 |
| Orange P3R | 10.65124 | 0.082181 | 0.8838 | 15.6011 | 19.37984 | 0.010362 | 0.9978 |
| Torque blue | 3.053515 | 0.046731 | 0.725 | 18.2904 | 19.08397 | 0.035842 | 0.9991 |
| Electrocoagulation time intervals after 120 min | | | | | | | |
| Foron ebl blue | 0.94973 | 0.019107 | 0.826 | 13.9457 | 14.28571 | 0.086855 | 0.9997 |
| Terasil brown | 3.423734 | 0.047191 | 0.8186 | 19.267 | 20.12072 | 0.056117 | 0.9978 |
| Orange P3R | 14.65548 | 0.091159 | 0.8787 | 16.7587 | 20.27171 | 0.007611 | 0.9979 |
| Torque blue | 3.053515 | 0.046731 | 0.8707 | 19.3845 | 20.20202 | 0.030037 | 0.9969 |

**Table 3.** *Cont.*

| Dyes | Pseudo First Order Kinetics | | | | Pseudo Second Order Kinetics | | |
|---|---|---|---|---|---|---|---|
| | $q_e$ (mg/g) Cal | $K_{1,ads}$ | $R^2$ | $q_e$ (mg/g) exp | $q_e$ (mg/g) | $K_{2,ads}$ | $R^2$ |
| **Electrocoagulation time intervals after 180 min** | | | | | | | |
| Foron ebl blue | 2.875411 | 0.04558 | 0.6214 | 15.91606 | 16.72241 | 0.036117 | 0.9978 |
| Terasil brown | 2.293507 | 0.048342 | 0.3587 | 19.3344 | 20.08032 | 0.044437 | 0.9996 |
| Orange P3R | 8.340652 | 0.075275 | 0.8146 | 17.569 | 19.80198 | 0.014567 | 0.9908 |
| Torque blue | 1.663796 | 0.024631 | 0.4924 | 19.8632 | 20.28398 | 0.056828 | 0.999 |

**Table 4.** Pseudo first and second order kinetics parameters of all dyes at 5 electrocoagulation time intervals (5, 10, 15, 20, 30 min) for every shaking time by calcinized composite.

| Dyes | Pseudo First Order Kinetics | | | | Pseudo Second Order Kinetics | | |
|---|---|---|---|---|---|---|---|
| | qe (mg/g) Cal | $K_1$,ads | $R^2$ | qe (mg/g) exp | qe (mg/g) | $K_2$,ads | $R^2$ |
| **Electrocoagulation time intervals after 30 min** | | | | | | | |
| Foron ebl blue | 1.570724 | 0.035451 | 0.2292 | 12.9432 | 13.51351 | 0.056796 | 0.999 |
| Terasil brown | 6.757717 | 0.066298 | 0.8794 | 15.74016 | 17.51313 | 0.017227 | 0.993 |
| Orange $P_3R$ | 7.120328 | 0.070441 | 0.8355 | 8.2 | 13.2626 | 0.010422 | 0.9859 |
| Torque blue | 4.983105 | 0.063075 | 0.8043 | 12.4096 | 14.0647 | 0.020893 | 0.9945 |
| **Electrocoagulation time intervals after 60 min** | | | | | | | |
| Foron ebl blue | 1.631924 | 0.030386 | 0.3308 | 13.588 | 14.08451 | 0.056654 | 0.9992 |
| Terasil brown | 5.556483 | 0.06952 | 0.7120 | 16.47232 | 18.11594 | 0.020705 | 0.9958 |
| Orange $P_3R$ | 10.03095 | 0.083102 | 0.8883 | 12.01256 | 18.58736 | 0.007411 | 0.9594 |
| Torque blue | 5.642869 | 0.065377 | 0.8424 | 13.9144 | 15.625 | 0.019432 | 0.993 |
| **Electrocoagulation time intervals after 90 min** | | | | | | | |
| Foron ebl blue | 2.340453 | 0.035911 | 0.7134 | 14.412 | 15.01502 | 0.042644 | 0.9979 |
| Terasil brown | 6.907168 | 0.070671 | 0.8690 | 17.53728 | 20.37984 | 0.017332 | 0.993 |
| Orange $P_3R$ | 9.89464 | 0.079649 | 0.8693 | 12.24408 | 16.6113 | 0.009786 | 0.9786 |
| Torque blue | 5.735879 | 0.060312 | 0.8831 | 15.4872 | 19.89189 | 0.019987 | 0.9927 |
| **Electrocoagulation time intervals after 120 min** | | | | | | | |
| Foron ebl blue | 1.588913 | 0.028545 | 0.3170 | 14.1256 | 14.59854 | 0.057211 | 0.9988 |
| Terasil brown | 5.663697 | 0.062845 | 0.6409 | 18.0032 | 19.41748 | 0.021089 | 0.9969 |
| Orange $P_3R$ | 13.03137 | 0.087246 | 0.8767 | 15.48536 | 22.66116 | 0.007715 | 0.9671 |
| Torque blue | 5.410034 | 0.062614 | 0.8932 | 16.64918 | 16.08318 | 0.021385 | 0.9962 |
| **Electrocoagulation time intervals after 180 min** | | | | | | | |
| Foron ebl blue | 2.198872 | 0.048572 | 0.2993 | 15.7728 | 14.59854 | 0.032246 | 0.9988 |
| Terasil brown | 5.430002 | 0.061694 | 0.8270 | 18.93504 | 19.28398 | 0.022101 | 0.9971 |
| Orange $P_3R$ | 9.088663 | 0.079879 | 0.8891 | 15.60112 | 18.45018 | 0.012665 | 0.9868 |
| Torque blue | 6.546362 | 0.067449 | 0.8396 | 18.01688 | 16.72387 | 0.018392 | 0.9957 |

### 3.8. Thermodynamic Studies

Temperature changes have two various effects on adsorption. Under pre-equilibrium conditions, the temperature can alter the rate of adsorption. Secondly, after attaining equilibrium, it changes the adsorption equilibrium position of the adsorbent for the adsorbate [45]. In this study, adsorption of Foron EBL dye, Terasil brown 2RFL, Torque blue, and Orange $P_3R$ using clay composites were investigated as a function of temperature. The experiment was performed at different temperatures, i.e., 30, 35, 40, 45, and 55 °C, and electrocoagulation was also performed combined with adsorption (Tables 5 and 6). When the temperature was raised from 30 to 55 °C (303 to 328 K), the amount of dye adsorbed decreased by treatment with both composites, consistent with the exothermic adsorption. The decrease is due to equilibrium shifting to desorption with the rise in temperature, and concomitant weakening of the adsorbate–adsorbent interactions also relate to it [45].

Thermodynamic parameters like enthalpy change ($\Delta H°$), entropy change ($\Delta S°$), and Gibbs free energy ($\Delta G°$) measure how the adsorption occurs from a thermodynamic viewpoint.

**Table 5.** Enthalpy change ($\Delta H$), Entropy change ($\Delta S$), and Gibbs free energy ($\Delta G$) for 4 dyes with non-calcinized composite.

| Dyes | T (Kelvin) | $\Delta G$ (kJmol$^{-1}$) | $\Delta H$ (J/mol) | $\Delta S$ (J mol$^{-1}$ K$^{-1}$) | $R^2$ |
|---|---|---|---|---|---|
| Orange P$_3$R | 303 | 7.381 | −8.4638 | −24.3938 | 0.9509 |
| | 308 | 7.503 | | | |
| | 313 | 7.625 | | | |
| | 318 | 7.747 | | | |
| | 328 | 7.991 | | | |
| Torque blue PG | 303 | 7.029 | −8.8605 | −23.233 | 0.7805 |
| | 308 | 7.145 | | | |
| | 313 | 7.262 | | | |
| | 318 | 7.378 | | | |
| | 328 | 7.61 | | | |
| Terasil brown 2RFL | 303 | 3.38 | −4.619 | −11.18 | 0.6429 |
| | 308 | 3.438 | | | |
| | 313 | 3.494 | | | |
| | 318 | 3.55 | | | |
| | 328 | 3.662 | | | |
| Foron ebl blue | 303 | 2.063 | −3.1669 | −6.8205 | 0.6285 |
| | 308 | 2.097 | | | |
| | 313 | 2.131 | | | |
| | 318 | 2.165 | | | |
| | 328 | 2.23 | | | |

**Table 6.** Enthalpy change ($\Delta H$), Entropy change ($\Delta S$), and Gibbs free energy ($\Delta G°$) using calcinized composite.

| Dyes | T (Kelvin) | $\Delta G$ (kJmol$^{-1}$) | $\Delta H$ (J/mol) | $\Delta S$ (J mol$^{-1}$ K$^{-1}$) | $R^2$ |
|---|---|---|---|---|---|
| Orange P$_3$R | 303 | 2.126 | −3.245 | −7.02973 | 0.9441 |
| | 308 | 2.160 | | | |
| | 313 | 2.196 | | | |
| | 318 | 2.231 | | | |
| | 328 | 2.302 | | | |
| Torque blue PG | 303 | 8.658 | −1.0704 | −28.5883 | 0.9244 |
| | 308 | 8.801 | | | |
| | 313 | 8.94 | | | |
| | 318 | 9.087 | | | |
| | 328 | 9.373 | | | |

**Table 6.** *Cont.*

| Dyes | T (Kelvin) | ΔG (kJmol$^{-1}$) | ΔH (J/mol) | ΔS (J mol$^{-1}$ K$^{-1}$) | R$^2$ |
|---|---|---|---|---|---|
| Terasil brown 2RFL | 303 | 3.791 | −5.5052 | −12.5358 | 0.6268 |
| | 308 | 3.853 | | | |
| | 313 | 3.916 | | | |
| | 318 | 3.979 | | | |
| | 328 | 4.1073 | | | |
| Foron ebl blue | 303 | 2.3405 | −3.8039 | −7.73755 | 0.5832 |
| | 308 | 2.379 | | | |
| | 313 | 2.417 | | | |
| | 318 | 2.456 | | | |
| | 328 | 2.533 | | | |

Best dyes adsorption using clay composites happens favorably at low temperatures. Negative values of $\Delta H^o$ showed the exothermic adsorption and dominated by physical processes in nature involving the weak attraction forces. Thermodynamic parameters are calculated to characterize the adsorption, such as standard enthalpy ($\Delta H^o$) and standard entropy change ($\Delta S^\circ$) due to the transfer of one-mole solute onto solid–liquid from the solution. Furthermore, Thermodynamic parameters suggest that the adsorption process is thermodynamically possible at room temperature but less at higher temperatures. Negative values of $\Delta S^\circ$ indicated the decrease in randomness at the interface of solid/solution with high temperature [25]. Similar results were obtained studying the adsorption of Congo red dye (CR) using clay material bentonite, kaolin, and zeolite, suggesting poor adsorption at the high temperature. This is due to the weakening physical interaction between the dye and adsorbent. The adsorption process was exothermic and spontaneous [46].

*3.9. SEM Analysis*

Scanning electron microscopy with TLD and ETD analysis was used to study the surface morphology of bentonite and zeolite-based composites. Figure 11a,b depicts the SEM micrographs at ×2500 magnifications for calcinized and non-calcinized composites, respectively. The micrographs obtained suggested that non-calcinized composite showed massive, aggregated, and coarse morphology. Bentonite-based adsorbent showed several pores with irregular shapes and rough and uneven surfaces. It exhibits a higher contact area and easy diffusion of pores during adsorption. Zeolite represents noticeable cage-like cavities having a surface with other impurities. The surface area and the porosity of the adsorbent are important parameters to determine its adsorption capacity and performance [47]. After calcination, pore volume and the surface area of bentonite-based adsorbent increased with a large number of small, separated flakes, as shown in Figure 11a. A large number of small, irregular empty cubes was also observed on the amorphous surface of the clay. A calcinized composite of bentonite clay and sodium zeolite showed many small particles scattered around the agglomerations and empty cubes. Due to enhanced surface area and porosity, calcinized composite is very efficient for dye removal. Modified bentonite showed similar results to SEM images for pollutants removal where calcination increased the porosity and surface area [48]. Similar results were obtained for unmodified bentonite clay, where massive plates with some phase separations are observed as heterogeneous surface morphology [49].

(**a**)                                                                                                (**b**)
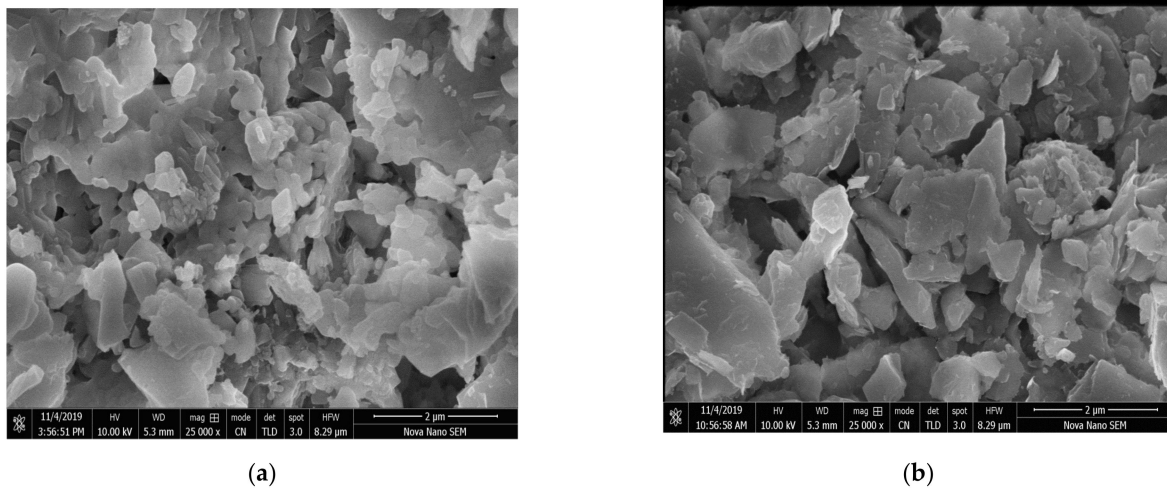
**Figure 11.** SEM images of (**a**) calcinized (**b**) non-calcinized composite of bentonite and sodium zeolite.

*3.10. FTIR Analysis*

The FTIR patterns of the calcinized composite of bentonite and sodium zeolite (Figure 12) exhibit several characteristic bands. In this track, different spectra have been observed, such as the Si–O–Al vibration at 510 cm$^{-1}$, Si–O bond stretching in 1040 cm$^{-1}$, Al–O and Si–O coupled out-of-plane bending vibrations at 680 cm$^{-1}$, octahedral layers represent in the range between 790 and 800 cm$^{-1}$. Range intensity has been reduced by calcinations, suggesting the displacement of water and silicon caused by thermal treatment [30].
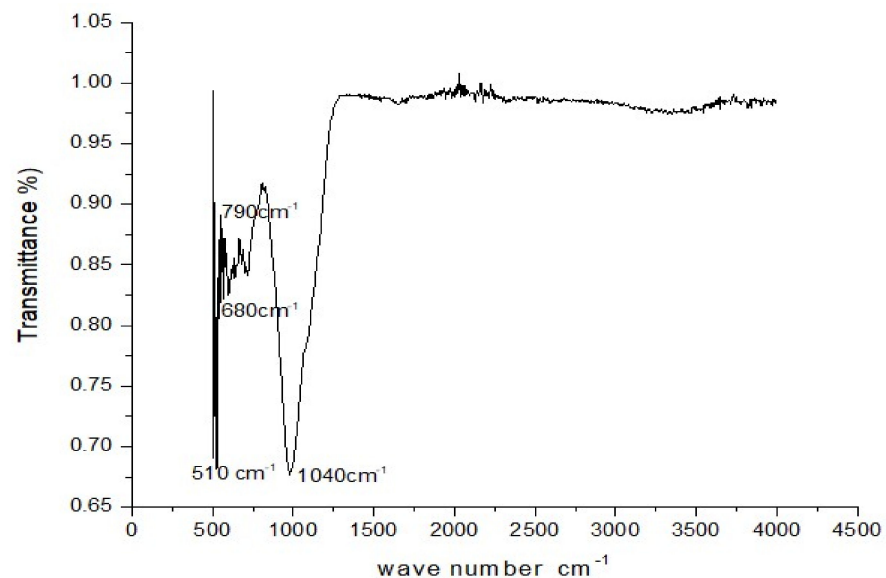


**Figure 12.** Infrared spectra of calcinized composite of bentonite and sodium zeolite.

In calcinized composite, the band at 1050 cm$^{-1}$ represents the symmetric stretching vibrations corresponding to SiO$_4$ or AlO$_4$ structure. This band is characteristic of the zeolitic framework structure. The spectra of the calcinized bentonite composite (Figure 12) did not show absorption bands at 1300 and 4000 cm$^{-1}$. After calcination, water OH-bending (1635 cm$^{-1}$) mode totally disappeared. This is a consequence of dehydroxylation and dehydration by thermal treatment [28]. Same vibrational bands have been observed in cobalt-based Brazilian bentonite [50].

## 4. Conclusions

The degradation of Foron EBL blue, Orange P$_3$R, Torque blue PG, and Terasil brown 2RFL dyes using a calcinized composite of bentonite and sodium zeolite as adsorbent is more efficient than non-calcinized material. Combining the adsorption process with electrocoagulation showed superior removal efficiencies for dye removal than using a single treatment. The maximum removal efficiency of Torque blue PG was 86.68%, followed by Terasil brown 2RFL (83.54%), Foron ebl blue (75.3%), and Orange P$_3$R (63.48%) by calcinized composite. Freundlich, Dubinin Radushkevich, and Harkin Jura isotherm models showed a somewhat better fit than the Langmuir and Temkin models for adsorption, suggesting that adsorption was onto a non-uniform and heterogonous surface. The fitting of experimental kinetic data indicated that the adsorption of all four dyes followed the pseudo-second-order kinetic model considering high $R^2$ values and the larger number of adsorption sites on the adsorbent surface. Thermodynamic studies indicated that adsorption is an exothermic reaction that takes place spontaneously in nature. SEM indicated the presence of porous structures on the heterogeneous and amorphous surface of clay-based composites, which can be efficiently utilized for dye adsorption. The good adsorption capacity, low cost, and thermodynamic stability of clay-based composites revealed that they could be used as effective adsorbents for water purification, and the environment can be preserved. The applicability of reusing the zeolite-based composite material for the removal of many pollutants, particularly phosphate, has vital importance on a commercial scale.

## References

1. Buonocore, E.; Mellino, S.; De Angelis, G.; Liu, G.; Ulgiati, S. Life Cycle Assessment Indicators of Urban Wastewater and Sewage Sludge Treatment. *Ecol. Indic.* **2018**, *94*, 13–23. [CrossRef]
2. Chopra, A.K.; Pathak, C. Accumulation of Heavy Metals in The Vegetables Grown in Wastewater Irrigated Areas of Dehradun, India with Reference to Human Health Risk. *Environ. Monit. Assess.* **2015**, *187*, 1–8. [CrossRef] [PubMed]
3. Robinson, T.; McMullan, G.; Marchant, R.; Nigam, P. Remediation of Dyes in Textile Effluent: A Critical Review on Current Treatment Technologies with A Proposed Alternative. *Bioresour. Technol.* **2001**, *77*, 247–255. [CrossRef] [PubMed]
4. Chu, W. Dye Removal from Textile Dye Wastewater Using Recycled Alum Sludge. *Water Res.* **2001**, *35*, 3147–3152. [CrossRef]
5. Vakili, M.; Rafatullah, M.; Salamatinia, B.; Abdullah, A.Z.; Ibrahim, M.H.; Tan, K.B.; Gholami, Z.; Amouzgar, P. Application of Chitosan and Its Derivatives as Adsorbents for Dye Removal from Water and Wastewater: A Review. *Carbohydr. Polym.* **2014**, *113*, 115–130. [CrossRef]
6. Ramesh, S.; Kim, H.S.; Sivasamy, A.; Kim, J.H. Synthesis of Octa (Maleimidophenyl) Silsesquioxane–Sio2/Tio2 Hybrid Nanocomposites: Adsorption Behavior for the Removal of an Organic Methylene Blue Dye and Antimicrobial Activity Against Pathogens. *Polym. Plast. Technol. Eng.* **2018**, *57*, 185–195. [CrossRef]
7. Pandit, P.; Basu, S. Removal of Organic Dyes from Water by Liquid–Liquid Extraction Using Reverse Micelles. *J. Colloid Interface Sci.* **2002**, *245*, 208–214. [CrossRef]
8. Khadhraoui, M.; Trabelsi, H.; Ksibi, M.; Bouguerra, S.; Elleuch, B. Discoloration and Detoxicification of a Congo Red Dye Solution by Means of Ozone Treatment for a Possible Water Reuse. *J. Hazard. Mater.* **2009**, *161*, 974–981. [CrossRef]

9. Sarkheil, H.; Tavakoli, J.; Behnood, R. Oil By-Product Removal from Aqueous Solution Using Sugarcane Bagasse as Absorbent. *Int. J. Emerg. Sci. Eng.* **2014**, *2*, 48–52.

10. Castañeda-Díaz, J.; Pavón-Silva, T.; Gutiérrez-Segura, E.E.; Colín-Cruz, A. Electrocoagulation-Adsorption to Remove Anionic and Cationic Dyes from Aqueous Solution by PV-Energy. *J. Chem.* **2017**, *2017*, 5184590. [CrossRef]

11. Brillas, E.; Martínez-Huitle, C.A. Decontamination of Wastewaters Containing Synthetic Organic Dyes by Electrochemical Methods. An Updated Review. *Appl. Catal. B Environ.* **2015**, *166*, 603–643. [CrossRef]

12. Mollah, M.Y.; Morkovsky, P.; Gomes, J.A.; Kesmez, M.; Parga, J.; Cocke, D.L. Fundamentals, Present and Future Perspectives of Electrocoagulation. *J. Hazard. Mater.* **2004**, *114*, 199–210. [CrossRef] [PubMed]

13. Vimonses, V.; Lei, S.; Jin, B.; Chow, C.W.; Saint, C. Adsorption of Congo Red by Three Australian Kaolins. *Appl. Clay Sci.* **2009**, *43*, 465–472. [CrossRef]

14. Queiroga, L.N.; Pereira, M.B.; Silva, L.S.; Filho, E.C.S.; Santos, I.M.; Fonseca, M.G.; Georgelin, T.; Jaber, M. Microwave ben-tonite silylation for dye removal: Influence of the solvent. *Appl. Clay Sci.* **2019**, *168*, 478–487. [CrossRef]

15. Mahmoodi, N.M.; Saffar-Dastgerdi, M.H. Zeolite Nanoparticle as a Superior Adsorbent with High Capacity: Synthesis, Surface Modification and Pollutant Adsorption Ability from Wastewater. *Microchem. J.* **2018**, *145*, 74–83. [CrossRef]

16. Zhang, G.; Qu, J.; Liu, H.; Liu, R.; Wu, R. Preparation and Evaluation of a Novel Fe–Mn Binary Oxide Adsorbent for Effective Arsenite Removal. *Water Res.* **2007**, *41*, 1921–1928. [CrossRef]

17. Şen, F.; Demirbaş, Ö.; Çalımlı, M.H.; Aygün, A.; Alma, M.H.; Nas, M.S. The Dye Removal from Aqueous Solution Using Polymer Composite Films. *Appl. Water Sci.* **2018**, *8*, 206. [CrossRef]

18. Aljeboree, A.M.; Alshirifi, A.N.; Alkaim, A.F. Kinetics and Equilibrium Study for the Adsorption of Textile Dyes on Coconut Shell Activated Carbon. *Arab. J. Chem.* **2017**, *10*, S3381–S3393. [CrossRef]

19. Pereira, I.D.S.; Silva, V.C.; Neto, J.F.D.; Neves, G.A.; Ferreira, H.C.; Menezes, R. Influence of the Purification of Bentonite Clay from New Deposits in the State of Paraíba-Brazil for Use in Water-Based Drilling Fluids. *Cerâmica* **2018**, *64*, 538–546. [CrossRef]

20. Wang, Y. Solar Photocatalytic Degradation of Eight Commercial Dyes in TiO2 Suspension. *Water Res.* **2000**, *34*, 990–994. [CrossRef]

21. Amin, M.T.; Alazba, A.A.; Shafiq, M. Adsorptive Removal of Reactive Black 5 from Wastewater Using Bentonite Clay: Isotherms, Kinetics and Thermodynamics. *Sustainability* **2015**, *7*, 15302–15318. [CrossRef]

22. Dada, A.; Olalekan, A.; Olatunya, A.; Dada, O. Langmuir, Freundlich, Temkin and Dubinin–Radushkevich Isotherms Studies of Equilibrium Sorption of Zn2+ Unto Phosphoric Acid Modified Rice Husk. *IOSR J. Appl. Chem.* **2012**, *3*, 38–45.

23. Khalil, M.; Hanif, M.A.; Rashid, U.; Ahmad, J.; Alsalme, A.; Tsubota, T. Low-Cost Novel Nano-Constructed Granite Com-Posites for Removal of Hazardous Terasil Dye from Wastewater. *Environ. Sci. Pollut. Res.* **2022**, 1–19. [CrossRef]

24. Ho, Y.S.; McKay, G.; Wase, D.A.J.; Forster, C.F. Study of the Sorption of Divalent Metal Ions on to Peat. *Adsorpt. Sci. Technol.* **2000**, *18*, 639–650. [CrossRef]

25. Vimonses, V.; Lei, S.; Jin, B.; Chow, C.; Saint, C. Kinetic Study and Equilibrium Isotherm Analysis of Congo Red Adsorption by Clay Materials. *Chem. Eng. J.* **2009**, *148*, 354–364. [CrossRef]

26. Zhao, X.; Hardin, I.R. HPLC and Spectrophotometric Analysis of Biodegradation of Azo Dyes by Pleurotus Ostreatus. *Dye. Pigment.* **2007**, *73*, 322–325. [CrossRef]

27. Mahmoud, M.; Farah, J.Y.; Farrag, T.E. Enhanced removal of Methylene Blue by Electrocoagulation Using Iron Electrodes. *Egypt. J. Pet.* **2013**, *22*, 211–216. [CrossRef]

28. Rejeb, R.; Antonissen, G.; De Boevre, M.; Detavernier, C.; Van de Velde, M.; De Saeger, S.; Ducatelle, R.; Ayed, M.H.; Ghorbal, A. Calcination Enhances the Aflatoxin and Zearalenone Binding Efficiency of a Tunisian Clay. *Toxins* **2019**, *11*, 602. [CrossRef]

29. Guo, Y.; Guo, Y.; Tang, D.; Liu, Y.; Wang, X.; Li, P.; Wang, G. Sol-Gel Synthesis of New Znfe2o4/Na-Bentonite Composites for Simultaneous Oxidation of Rhb and Reduction of Cr (VI) Under Visible Light Irradiation. *J. Alloy Compd.* **2019**, *781*, 1101–1109. [CrossRef]

30. dos Santos, F.R.; de Oliveira Bruno, H.C.; Melgar, L.Z. Use of Bentonite Calcined Clay as An Adsorbent: Equilibrium and Ther-Modynamic Study of Rhodamine B Adsorption in Aqueous Solution. *Environ. Sci. Pollut. Res.* **2019**, *26*, 28622–28632. [CrossRef]

31. Islam, A.; Guha, A.K. Removal of pH, TDS and Color from Textile Effluent by Using Coagulants and Aquatic/Non-Aquatic Plants as Adsorbents. *Resour. Environ.* **2013**, *3*, 101–114.

32. Rusdianasari, R.; Bow, Y.; Yuniar, Y. Treatment of Traditional Cloth Wastewater by Electrocoagulation Using Aluminum Elec-Trodes. *Int. J. Adv. Sci. Eng. Inf. Technol.* **2014**, *4*, 99–104. [CrossRef]

33. Kumar, P.S.; Ramalingam, S.; Senthamarai, C.; Niranjanaa, M.; Vijayalakshmi, P.; Sivanesan, S. Adsorption of Dye from Aqueous Solution by Cashew Nutshell: Studies on Equilibrium Isotherm, Kinetics and Thermodynamics of Interactions. *Desalination* **2010**, *261*, 52–60. [CrossRef]

34. Ozdes, D.; Duran, C.; Senturk, H.B.; Avan, H.; Bicer, B. Kinetics, Thermodynamics, and Equilibrium Evaluation of Adsorptive Removal of Methylene Blue onto Natural Illitic Clay Mineral. *Desalin. Water Treat.* **2013**, *52*, 208–218. [CrossRef]

35. Shamsudin, M.S.; Azha, S.F.; Shahadat, M.; Ismail, S. Cellulose/Bentonite-Zeolite Composite Adsorbent Material Coating for Treatment of N-Based Antiseptic Cationic Dye from Water. *J. Water Process. Eng.* **2019**, *29*, 100764. [CrossRef]

36. Inyinbor, A.A.; Adekola, F.A.; Olatunji, G.A. Kinetics, Isotherms and Thermodynamic Modeling of Liquid Phase Adsorption of Rhodamine B Dye onto Raphia Hookerie Fruit Epicarp. *Water Resour. Ind.* **2016**, *15*, 14–27. [CrossRef]

37.　Arivoli, S.; Henkuzhali, M. Kinetic, Mechanistic, Thermodynamic and Equilibrium Studies on the Adsorption of Rhodamine B by Acid Activated Low-Cost Carbon. *E J. Chem.* **2008**, *5*, 187–200. [CrossRef]

38.　Foo, K.Y.; Hameed, B.H. Insights into the Modeling of Adsorption Isotherm Systems. *Chem. Eng. J.* **2010**, *156*, 2–10. [CrossRef]

39.　Loukidou, M.X.; Zouboulis, A.I.; Karapantsios, T.D.; Matis, K.A. Equilibrium and Kinetic Modeling of Chromium (VI) Biosorp-Tion by Aeromonas Caviae. *Colloids Surf. A Physicochem. Eng. Aspects.* **2004**, *242*, 93–104. [CrossRef]

40.　Bhatti, H.N.; Noreen, S.; Tahir, N.; Ilyas, S.; Siddiqua, U.H. Equilibrium, Thermodynamic and Kinetic Studies for Biosorption of Terasil Brown 2RFL From Contaminated Water Using Economical Biomaterial. *Mediterr. J. Chem.* **2015**, *4*, 239–251. [CrossRef]

41.　Sun, Q.; Hu, X.; Zheng, S.; Sun, Z.; Liu, S.; Li, H. Influence of Calcination Temperature on the Structural, Adsorption and Pho-Tocatalytic Properties of Tio2 Nanoparticles Supported on Natural Zeolite. *Powder Technol.* **2015**, *274*, 88–97. [CrossRef]

42.　Liu, Q.; Li, T.; Zhang, S.; Qu, L.; Ren, B. Optimization and Evaluation of Alkali-Pretreated Paeonia Ostii Seed Coats as Adsorbent for the Removal of Mb from Aqueous Solution. *Pol. J. Chem. Technol.* **2018**, *20*, 29–36. [CrossRef]

43.　Özcan, A.S.; Erdem, B.; Özcan, A. Adsorption of Acid Blue 193 from Aqueous Solutions Onto BTMA-Bentonite. *Colloids Surf. A Physicochem. Eng. Asp.* **2005**, *266*, 73–81. [CrossRef]

44.　Vimonses, V.; Jin, B.; Chow, C.W. Insight into Removal Kinetic and Mechanisms of Anionic Dye by Calcined Clay Materials and Lime. *J. Hazard. Mater.* **2010**, *177*, 420–427. [CrossRef] [PubMed]

45.　Shikuku, V.O.; Zanella, R.; Kowenje, C.O.; Donato, F.F.; Bandeira, N.M.; Prestes, O.D. Single and Binary Adsorption of Sul-Fonamide Antibiotics onto Iron-Modified Clay: Linear and Nonlinear Isotherms, Kinetics, Thermodynamics, And Mechanistic Studies. *Appl. Water Sci.* **2018**, *8*, 175. [CrossRef]

46.　Singh, K.P.; Mohan, D.; Sinha, S.; Tondon, G.; Gosh, D. Color removal from wastewater using low-cost activated carbon de-rived from agricultural waste material. *Ind. Eng. Chem. Res.* **2003**, *42*, 1965–1976. [CrossRef]

47.　Akl, M.; Youssef, A.; Al-Awadhi, M. Adsorption of Acid Dyes onto Bentonite and Surfactant-Modified Bentonite. *J. Anal. Bioanal. Technol.* **2013**, *4*, 3–7.

48.　Hua, J. Synthesis and Characterization of Bentonite Based Inorgano–Organo-Composites and Their Performances for Removing Arsenic from Water. *Appl. Clay Sci.* **2015**, *114*, 239–246. [CrossRef]

49.　Abdullahi, S.; Audu, A. Comparative Analysis on Chemical Composition of Bentonite Clays Obtained from Ashaka and Tango Deposits in Gombe State, Nigeria. *ChemSearch J.* **2017**, *8*, 35–40.

50.　Cótica, L.; Freitas, V.; Santos, I.; Barabach, M.; Anaissi, F.; Miyahara, R.; Sarvezuk, P. Cobalt-Modified Brazilian Bentonites: Preparation, Characterisation, and Thermal Stability. *Appl. Clay Sci.* **2010**, *51*, 187–191. [CrossRef]